# Laser absorption spectroscopy on a transient aluminum plasma generated by excimer laser ablation

C. Ursu, P. Nica, G.B. Rusu, C. Vitelaru, Gh. Popa, Cristian Focsa

# Laser absorption spectroscopy on a transient aluminum plasma generated by excimer laser ablation

**C. Ursu[1,2], P. Nica[3,*], G. B. Rusu[1], C. Vitelaru[2,4], Gh. Popa[2] and C. Focsa[5]**

[1] *"Petru Poni" Institute of Macromolecular Chemistry, 41 A Gr. Ghica Voda Alley, Iasi 700487, Romania*
[2] *Faculty of Physics, "Alexandru Ioan Cuza" University of Iasi, Blvd. Carol I, Nr.11, Iaşi 700506, Romania*
[3] *Department of Physics, "Gheorghe Asachi" Technical University, Iasi, 700050, Romania*
[4] *National Institute of Research and Development for Optoelectronics–INOE 2000, 409 Atomistilor Str., 051431 Magurele-Bucharest, Romania*
[5] *Univ. Lille, CNRS, UMR 8523, PhLAM – Physique des Lasers, Atomes et Molécules, F-59000 Lille, France*

**Corresponding author*: pnica@tuiasi.ro

**Abstract:**

Transient Al plasma produced by excimer laser ablation in vacuum was investigated through laser absorption spectroscopy to probe the space-time evolution of neutral species. Spectrally integrating the absorbance, the ground state Al atoms column density was calculated. Typical decreasing trends in time (over a plasma lifetime of about 10 μs) and space (for distances in the range 0.5 – 8.5 mm from the target surface) were observed. The kinetic temperature of Al ground state species was also estimated from the recorded linewidths, in the assumption of a Doppler broadening mechanism. The resulted values displayed only weak time-fluctuations, while the time-averaged ones showed. a significant drop in few millimeters from the target, similarly to the column density behavior.

**Keywords**: Excimer laser ablation, Aluminum plasma, Absorption spectroscopy, Laser-produced transient plasma, Plasma dynamics

## 1. Introduction

Thorough investigation of Laser Induced Plasma (LIP) dynamics is of paramount importance for providing better understanding of the complex physical processes occurring in the plasma plume, and also for optimizing various practical applications of laser ablation such as pulsed laser deposition [1], nanoparticle synthesis [2], higher harmonic[3] or extreme ultraviolet radiation generation [4]. Among various experimental methods available, the optical emission spectroscopy (OES) [5] is one of the most used, due to its implementation easiness and non-invasiveness. However, OES cannot give (direct) access to ground state populations, and it is generally limited to the early stages of the plume expansion, because of the relatively short plasma emission lifetime. Alternatively, the investigation of LIP parameters by laser absorption spectroscopy (LAS) provides detailed information on the basic plasma processes and it has become a versatile tool for its diagnosis [6–11]. Combining OES and LAS, a more comprehensive characterization of the plasma over its entire lifetime is possible, leading to a better understanding of its behavior [12–14]. Dual-laser photo-absorption [15] and Fraunhofer-type absorption [16] methods were also proposed for detailed time- and space-investigation of LIP.

LAS offers the opportunity to precisely measure a significant number of plasma parameters, such as the number density of a given species, which makes it useful for, e.g., controlling the deposition process of thin films [6]. By using tunable lasers with narrow linewidths, the method is not affected by the instrumental broadening (as in the case of optical emission spectroscopy), and therefore provides high spectral resolution. When assuming a prevalent Doppler broadening mechanism, the kinetic temperature and path-integrated density of given species can be deduced from the profiles of the recorded spectral lines. Beside the fundamental scope, such plasma diagnostics may lead to great practical applications, e.g. isotopic ratio measurements from spectral shifting [17]: several elements were analyzed in this manner, such as uranium [18,19], plutonium [20], rubidium [21], strontium [22], gadolinium [23].

A “universal” application of the LAS method requires narrow-band widely tunable UV-VIS lasers, which are still quite expensive and cumbersome systems. Some studies even developed extreme-ultraviolet absorption spectroscopy in dual plasma schemes [24], which proved to be powerful tools for the study of photo-absorption in refractory atoms and along isonuclear/isoelectronic sequences, but the experimental implementation of these laser-plasma continua is yet cumbersome. The development of tunable diode lasers (TDL), with improved stability and considerably lower cost compared to broadband tunable lasers, fostered the wide-scale application of the absorption spectroscopy for LIP characterization. A large variety of laser diodes is now available, with multi-nm tunable range and sub-pm typical emission linewidth, e.g., AlGaInP (630 nm, 670 nm, 680 nm, 690 nm), AlGaAs (780nm, 830 nm), InGaAs (980 nm), etc [7–9]. Although the “universal” character is lost (i.e. all species in an LIP cannot be probed with a single laser source), the combined use of several TDLs, tuned on the main absorption features of the plume constituents, can still be an appealing, lower cost and easier implementation solution for LAS in laser-produced transient plasmas.

Continuing a series of systematic investigations on LIP dynamics, by optical (OES, ICCD imaging) [25,26] and electrical (Langmuir, electrostatic energy analyzer, target current measurement, etc.)[27–29] methods, we report here our first LAS study on the thoroughly characterized Aluminum LIP. These measurements are complementary of OES and can contribute to getting the full picture of the complex plasma dynamics [11]. Transient plasma is generated in vacuum by excimer laser ablation of Al and a blue TDL is used to probe the space-time evolution of neutral species. By tuning the laser diode wavelength in the range 394.393–394.407 nm, the spectral absorption profile of the Al I $3s^2\,3p\,(^2S_{1/2}) - 3s^2\,4s\,(^2P_{1/2})$ line is recorded, and subsequent estimations of plasma temperature and ground state Al atom density are derived.

## 2. Experimental Method and Setup

The experimental setup is shown in Figure 1. A laser diode emitting at ~394.4 nm (Toptica DL100, spectral width ~ 1 MHz, tunable between 394.393 nm and 394.407 nm) is used to study the plasma produced by excimer laser ablation (XeCl 308 nm, 45° incidence angle, 20 ns pulse width, 45 mJ pulse energy) of an aluminum target (99.9% purity) placed in a vacuum chamber ($10^{-6}$ Torr), for a laser irradiance of about 130 MW/cm$^2$. The LAS set-up includes a Fabry-Perot interferometer (FPI 100, 1 GHz free spectral range), a 0.001 nm resolution wavemeter (WaveMaster, Coherent), a 2 GHz oscilloscope (LeCroy WaveRunner 6200A). The interferometer was preliminary used for the measurement and the monitoring of the radiation emitted by the laser diode. It was ensured that the wavelength variation is continuous, in a spectral range of ~14 pm.

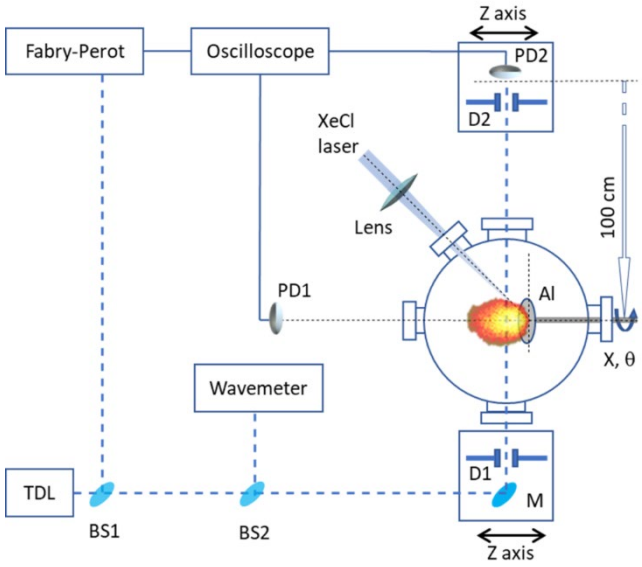


Figure 1: LAS experimental setup used for the Al LIP investigation (TDL - tunable diode laser, BS1, BS2 – beam splitters, M – mirror, D1, D2 – diaphragms, PD1, PD2 - photodiodes).

Two fast photodiodes are connected to the oscilloscope (Figure 1): PD1 (Thorlabs DET210, 1 ns rise time) records the plasma optical emission to use it as a triggering signal, while PD2 (Thorlabs DET210, 1 ns rise time) receives the TDL beam after passing through the LIP. A circular spot of 0.5 mm diameter was selected from the elliptic cross section shape of the diode laser beam (whose main axes were 3 mm and 1 mm, respectively) by using the D1 diaphragm. To minimize the contribution of the plasma emission ($I_{plasma}$) to the recorded signal, the PD2 photodiode was placed ~1 m away from the vacuum chamber, with an additional 3 mm diaphragms (D2) placed along the laser path. When the TDL is switched off, only $I_{plasma}$ is recorded; when the TDL beam is switched on, the optical intensity signal recorded by PD2 is:

$$I_{PD2} = I_t + I_{plasma} \tag{1}$$

where $I_t$ is the intensity of the TDL beam after crossing the plasma plume, which follows the Beer – Lambert law:

$$I_{PD2} - I_{plasma} = I_0 e^{-k_\lambda L} \tag{2}$$

where $I_0$ is the intensity of the TDL beam in absence of plasma plume, $k_\lambda$ is the linear absorption coefficient at the $\lambda$ wavelength, and $L$ is the absorption length which is time- and space-dependent. In fact, in the case of transient plasmas it is necessary to see the product $k_\lambda L$ as an integral $A(\lambda,t) = \int k_\lambda(x,t)\,dx$ along the laser absorption path in plasma, where $A(\lambda,t)$ is the spectral absorbance which is also time dependent.

Two micrometric precision positioning systems are used to translate the M mirror (together with the D1 diaphragm) and the PD2 photodiode (together with the D2 diaphragm) along the Z axis (which is the plasma plume axis of symmetry). This allows scanning the TDL beam through the LIP at various Z distances (in the range 0.5 – 8.5 mm) from the Al target surface, and thus performing space-resolved measurements of the plasma parameters.

The present study is focused on the determination of the absorption profile of the neutral aluminum atoms corresponding to the optical transition Al I $3s^2\,3p\ (^2S_{1/2}) - 3s^2\,4s\ (^2P_{1/2})$ at 394.401 nm. The nuclear spin – electron angular momentum interaction causes a hyperfine splitting, consisting in four components of relative intensities $32:27:9:32$ and frequency shifts with respect to the unperturbed transition frequency: $-1506$ MHz: 0 MHz: 0 MHz: $+1506$ MHz (Figure 2).

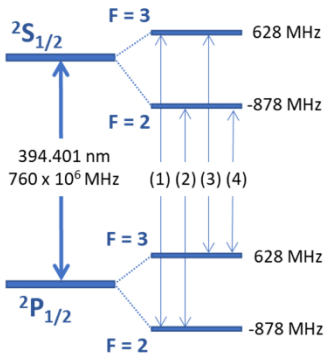


Figure 2: Al I 394.401 nm spectral line energy level diagram: hyperfine shifts and transitions (1-4).

## 3. Experimental results

### *3.1. Space-time resolved spectral absorption profile*

Figure 3 displays the typical time-evolution of the transmitted light intensity and the corresponding absorbance, for the resonance wavelength of Al I line at 394.401 nm. This result

emphasizes the presence of ground state Al atoms in two plasma structures (coined as "fast" and "slow"), which confirms previous results obtained by our group using OES and Langmuir probe measurements [28,30] and by other groups using various techniques [31–33]. The fast structure population is recorded in the first microsecond after the initiation of the ablation plume, whereas the slow one is delayed, with a maximum at 2.5 μs and a tail that lasts beyond 10 μs. Such plasma structures, often reported in literature [31,34–36], usually consist in a fast (hot) part dominated by highly charged particles ejected at early moments, accelerated through the electric field generated by the charge separation, and a tail of slow (cold) particles (of lower average charge state) ejected through subsequent thermal mechanisms[29,30,37]. Although the optical emission spectroscopy studies show a prevalence of excited neutral atoms in the second (slow) structure (whereas the fast structure is characterized by the presence of ions), these two observations are not contradictory, as the ground state neutral atoms in the first (fast) structure could come from (radiative) recombination processes.

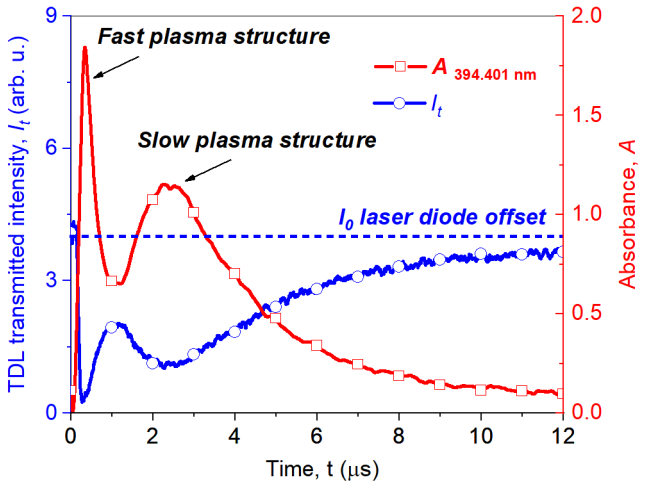


Figure 3: Typical time-evolution of the TDL transmitted intensity ($I_t$) and the corresponding absorbance ($A$), for the Al I spectral line at 394.401 nm (at 0.5 mm from the target surface).

To reconstruct the absorption spectral profile, we further tuned the laser diode emission wavelength over the range 394.393 ÷ 394.407 nm in 1 pm steps. Following the procedure described in Section 2, the spectral absorbance temporal evolution was recorded for each wavelength at various Z distances from the target, resulting in a (time, wavelength) matrix for each Z. Using the temporal variation along a matrix line and the wavelength variation along a column, one can derive contour plots as the ones displayed in Figure 4. We note that each plot was scaled to its maximum absorbance value for a better observation of the plasma evolution, whilst the total plasma absorbance is obviously decreasing in time. In the upper and lateral graphs associated with each contour plot, typical time-evolution at various wavelengths and spectral profiles at specific times are also traced (in correspondence with the dotted horizontal and vertical lines from the contour plot).

Let us notice that the spectral absorption profiles are well defined around the resonant peak center (394.401 nm) only at later times, after ~1.5 μs from the ablation laser pulse, *i.e.* for the second plasma structure. Since the experiments were performed in vacuum, for early times the Doppler splitting is seen as central dip in the absorption profiles, at 0.35 μs (Figure 4a), 0.45 μs (Figure 4b), 0.6 μs (Figure 4c), 0.75 μs (Figure 4d) and 0.9 μs (Figure 4e), because of the counter-propagating velocity distributions of atoms along the probe laser line of sight. Also, for short delays we do not observe a typical absorption profile (in the form of a classical Gaussian or Voigt function), the recorded broadening being most probably due to the addition of various processes: Stark and Doppler [18,22,38] broadening (see below), continuum emission (Bremsstrahlung) or absorption (inverse Bremsstrahlung) by free electrons in the plasma, and even possible probe beam deflection due to the modified refractive index [39]. The key point is finally the reduction of lower state population at higher temperature conditions according to Boltzmann distribution (see Figure 10 of [40]). Considering this complexity at very early times of the plasma plume propagation, the present study will be mainly focused on the later stages (> 2 μs) of the plasma evolution.

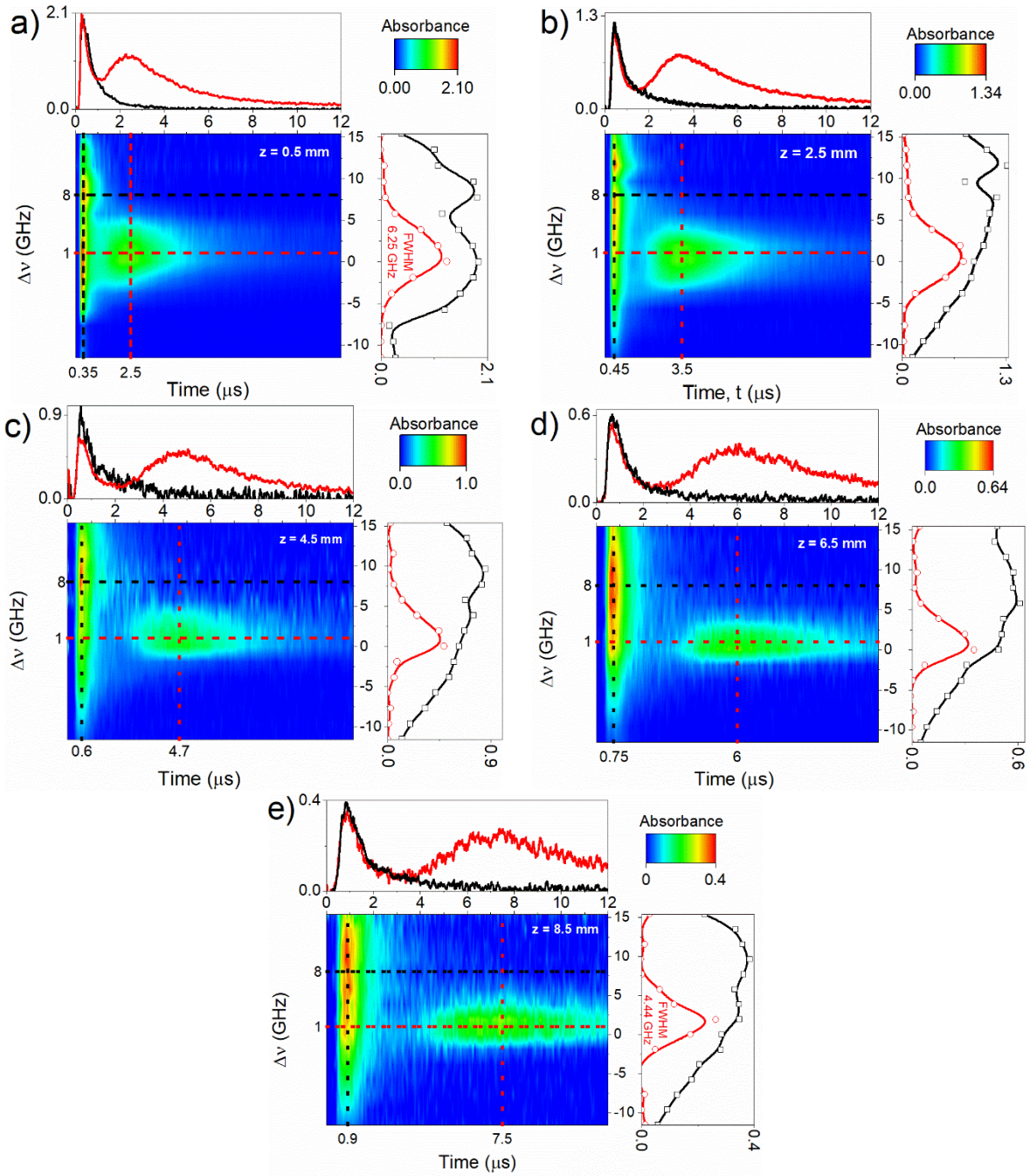


Figure 4: Time evolution of the path-integrated spectral absorption coefficient at various distances from the target: $z$ = 0.5 mm (a), $z$ = 2.5 mm (b), $z$ = 4.5 mm (c), $z$ = 6.5 mm (d), $z$ = 8.5 mm (e); the profiles corresponding to horizontal and vertical cross-sections of each determined contour map denote the temporal variation of the absorption coefficient determined within the laser diode spectral range and the obtained laser absorption profile at various delays from the laser ablation pulse, respectively.

Let us further focus on the space-time evolution of the maximum absorption at 394.401 nm. When moving away from the target surface, *i.e.* increasing the Z distance, the two local maxima (associated with the fast and slow plasma structures, Figure 5a) shift towards longer time delays, showing a linear space-time evolution (Figure 5b) One can thus derive the expansion velocities of the two structures, which are $v_{fast} = 1.57\times10^4$ m/s and $v_{slow} = 1.63\times10^3$m/s, in excellent agreement with values previously measured by various methods, such as plasma imaging [25,28,30], optical emission spectroscopy[41] or electrical plasma diagnostics [27,42].

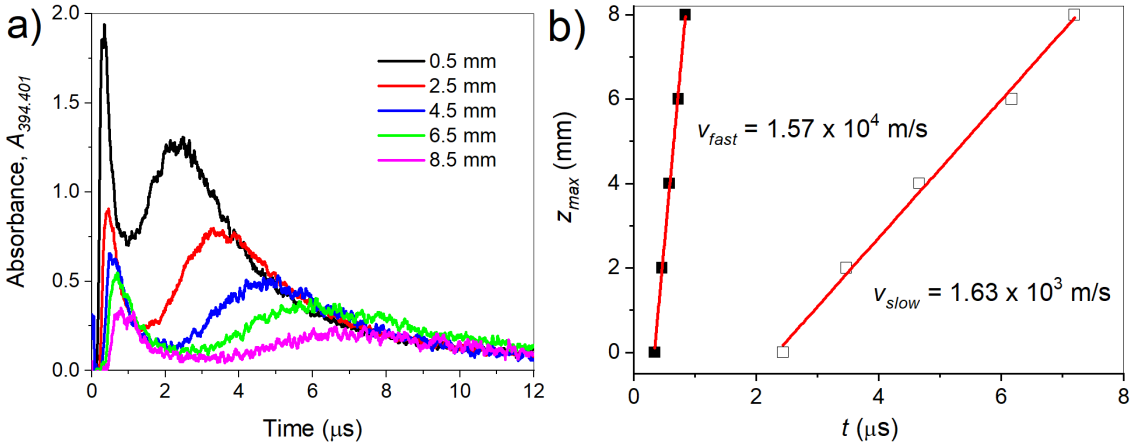


Figure 5: Temporal evolution of the 394.401 nm absorbance at various distances from the target surface (a), and space-time evolution of the maximum absorbance (b), used to calculate the fast and slow structures velocities.

*3.2. Density and temperature evolution*

In order to determine the space-time evolution of the ground state Al atoms density and kinetic temperature, we further focus on the well-defined absorption spectral profiles recorded at delays higher than 2 μs from the laser pulse (*i.e.* not affected by the continuum absorption at early expansion times, see above). By spectrally integrating the absorbance over the recorded line profiles, the path-integrated number density of the neutrals in the lower state (column density) $n_0 L$ can be calculated using [43–45]:

$$\int A(\nu, t)\, d\nu = 2.654 \times 10^{-6} [m^2/s] \cdot f_{12} n_0 L, \qquad (3)$$

where $f_{12} = 0.116$ is the oscillator strength of the considered transition [46], $n_0$ is the number density of the lower (ground) state, and $L$ is the path length.

The resulting time evolution of the column density is given in Figure 6, for several distances from the target. As expected, a decrease is observed (after an initial fast transient increase) over a plasma lifetime of about 10 μs. When moving away from the target surface, the maximum value decreases from ~$2.5 \cdot 10^{11}$ cm$^{-2}$ at $z$=0.5 mm to $0.5 \cdot 10^{11}$ cm$^{-2}$ at $z$=8.5 mm. Thus, by considering typical values of millimetres for the absorption path, it results an order of magnitude of $10^{12}$ cm$^{-3}$ for the neutral density in the ground state. This is in agreement with values obtained by other authors when using LAS to characterize low-temperature and low-density plasma plumes [45,47], as particularly obtained for LIP at longer expansion times. We also note that measurements performed by various (electrical, OES) methods on the second (slow) plasma structure (at few microseconds from the laser pulse) led to same order of magnitude densities for the charged particles (see, e.g.,[48,49]). This is the typical case of a few eV temperature plasma, where fractional populations of species can be estimated from well-known models as collisional radiative or local thermodynamic equilibrium [50,51].

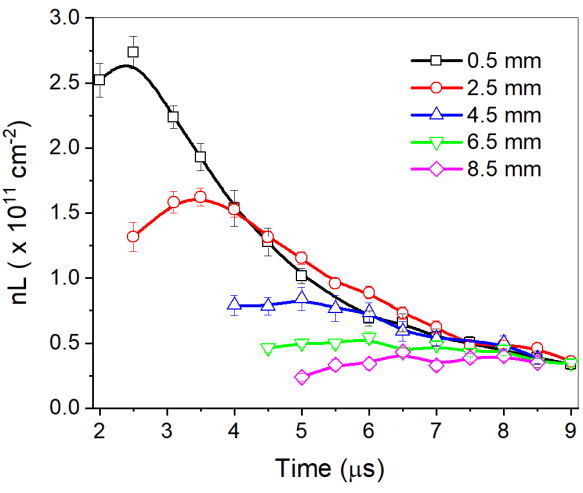

Figure 6: The time evolution of the neutral Al (in the ground state) column density for the second plasma structure at various distances from the target surface. The error bars are calculated with Eq. (3) from standard deviations of integrated peak areas, returned by the numerical fitting of the absorption profiles using a Gaussian function.

The Stark and the Doppler mechanisms have the major roles in LIP spectral line broadening [52–55]. The Stark effect is dominant at early expansion times, when the electron number density and the local electric field are high. At later times (microseconds) of plasma evolution, the Doppler broadening through thermal motion of the absorbing species will become dominant. In a previous paper [56] we used OES and the Stark-broadening and shifting of the 833.5 nm neutral carbon line for electron density evaluations. Values in the range of $10^{18}$ cm$^{-3}$ were derived for early stages, followed by an exponential decay with a time constant of about 60 ns. Then, by plotting the line width *vs*. central wavelength, a linear dependence resulted, confirming the negligible ion collisions contribution to the broadening/shifting mechanism. In the present case of Al plasma and 394.401 nm line, according with [53,57], for $N_e$=1.42×10$^{17}$ cm$^{-3}$, it was theoretically estimated $\Delta\lambda_{1/2}$ =0.462 Å and $\lambda_{shift} = 0.14$ Å at $T$=9670 K, while for $T$=13200 K, it resulted $\Delta\lambda_{1/2} = 0.54$ Å, and $\lambda_{shift} = 0.31$ Å. For the results of our measurements given in Figure 3, we are focused on the later stages of plasma expansion, when the line profile of neutral Al centered at 394.401 nm is clearly defined. According to the data given in Figure 6, for delays longer than 2 μs the local density (and consequently the local electric field) is lower with few orders of magnitude, allowing to neglect the Stark effect, similarly as in [12]. Thus, in the framework of the Doppler broadening mechanism, the kinetic temperature $T$ of the neutral Al atoms can be estimated by measuring the full width at half maximum (FWHM) of the recorded spectral profiles $\Delta\nu$ through the relationship [58,59]:

$$T = \frac{\lambda_0^2 m_a}{8kln2}\Delta\nu^2, \quad (4)$$

where $\lambda_0$ is the line center wavelength, $m_a$ the mass of an Al atom, and $k$ the Boltzmann constant. This assumes a Maxwell velocity distribution function which gives a Gaussian spectral profile.

To account for the hyperfine splitting (see Figure 2), the transmitted photodiode signal is often numerically fitted with a sum of four Doppler line profiles [60–62]. Such procedure was also applied in our analysis, by considering the relative intensities and frequency shifts given above, while the same width of the line profiles was assumed. Our estimations for the line widths indicate only weak time-fluctuations (in the determination error limits), for all the analyzed distances. In such circumstances, the experimentally-recorded line profiles were averaged for the relevant time-ranges (Figures 7a), in correspondence with Figures 4a)-e), when the absorption in the slow plasma structure manifests, as follows: [1.5 - 5.0] μs – at 0.5 mm, [2.0 - 6.0] μs – at 2.5 mm, [3.0 - 8.0] μs – at 4.5 mm, [4.0 - 10.0] μs – at 6.5 mm, and [4.5 - 12.0] μs – at 8.5 mm from the target surface. Figure 7a displays the comparison of the time-averaged experimental data points and the fitting spectral profile as a weighted sum of the four hyperfine components of relative intensities $32:27:9:32$.

The time-averaged kinetic temperatures were further numerically estimated using Eq. (4), and they are plotted in Figure 7b in comparison with the density space-evolution. Similar behavior can be observed, with a significant decrease within millimeters from the target surface. The values are in good agreement with prior measurements on the Al I 394.4 nm transition [45]. We finally notice that in the frame of the local thermodynamic equilibrium model (collision-dominated plasma) [50], the temperatures deduced from emission/absorption/vibrational/rotational spectra should be the same at a given point in space/time. However, even if the McWhirter criterion [63] is usually fulfilled [12,64] at short distances/delays from the target/laser pulse, the validity of LTE is questionable particularly at farther distances from the target or at later times of plasma evolution (not collision dominated) and hence further research efforts are necessary for a proper comparison.

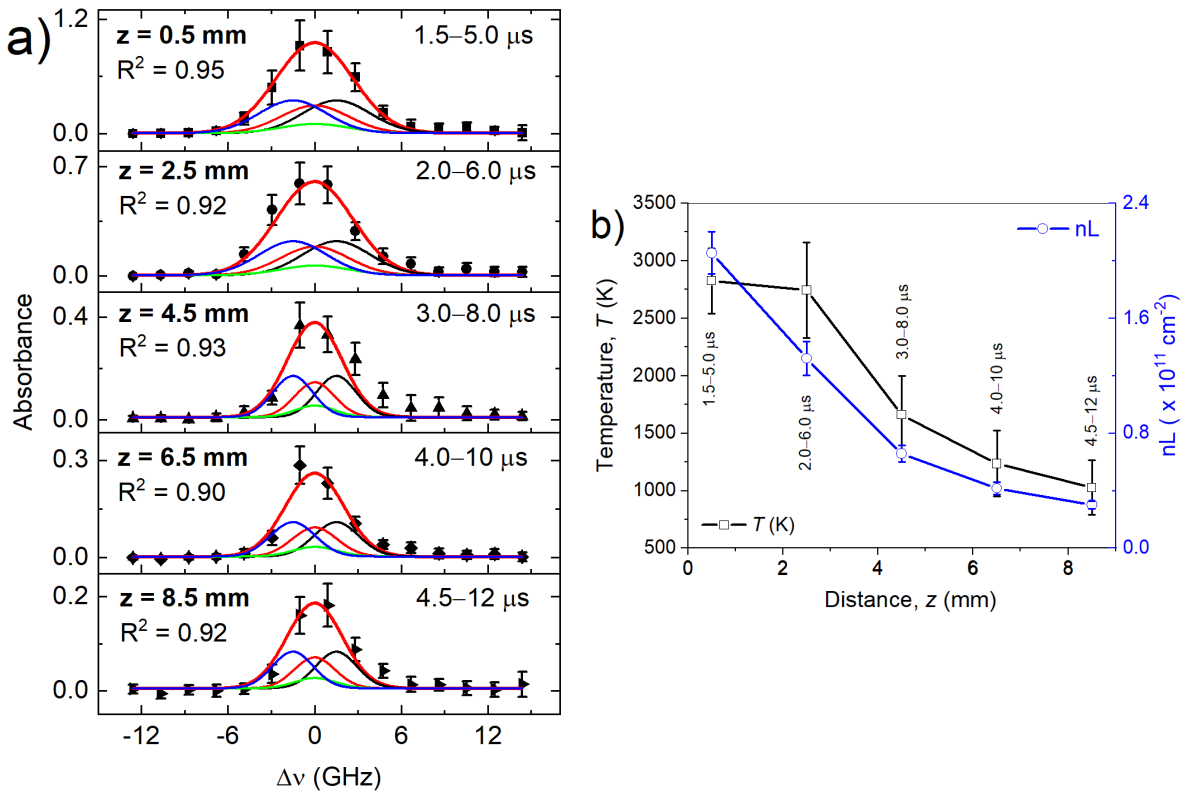


Figure 7: The averaged absorption profiles in the relevant time-ranges for to the slow plasma structure (a) and the evolution of the average kinetic plasma temperature and of the column density with the distance from the target (b). The error bars are standard deviations of the time-averaging (a) or of the parameters calculated with Eqs. (3) and (4) after numerical fitting of the absorption profiles (b).

**4. Conclusion**

A transient Al plasma produced by excimer laser ablation in vacuum was investigated through laser absorption spectroscopy. Using a tunable blue laser diode (in the range 394.393 nm – 394.407 nm) the space-time evolution of the neutral species was monitored from the spectral absorption profiles of the resonant transition $^2S_{1/2} \leftrightarrow {}^2P_{1/2}$ at 394.401 nm. The temporal evolution of the maximum absorption at 394.401 nm displays two local maxima, regardless of the distance from the target surface, assigned to two distinct plasma structures (fast and slow). From the linear position *vs.* time evolution of these two maxima, the expansion velocities of the two structures ($v_{fast} = 1.57\times10^4$ m/s and $v_{slow} = 1.63\times10^3$m/s) were derived.

The space-time evolution of the ground state Al atoms column density was studied by spectrally integrating the absorbance, showing typical decreasing trends in time (over a plasma lifetime of about 10 µs) and space (for distances in the range 0.5 – 8.5 mm from the target surface). A $10^{12}$ cm$^{-3}$ order of magnitude was estimated for the number density, in agreement with previous literature results.

In the assumption of a Doppler broadening mechanism, the kinetic temperature of Al ground state species was estimated from the width of the spectral profiles. Since only weak time-fluctuations (in the determination error limits) were obtained for all the analyzed distances, the time-averaged kinetic temperatures were computed. Similar space-dependence with column density was observed, with a significant decrease over few millimeters from the target surface.

**References**


[1] D.H. Lowndes, D.B. Geohegan, A.A. Puretzky, D.P. Norton, C.M. Rouleau, Synthesis of novel thin-film materials by pulsed laser deposition, Science (80-. ). 273 (1996) 898–903. https://doi.org/10.1126/science.273.5277.898.

[2] G. Ausanio, S. Amoruso, A.C. Barone, R. Bruzzese, V. Iannotti, L. Lanotte, M. Vitiello, Production of nanoparticles of different materials by means of ultrashort laser pulses, Appl. Surf. Sci. 252 (2006) 4678–4684. https://doi.org/10.1016/j.apsusc.2005.07.089.

[3] C. Thaury, F. Quéré, High-order harmonic and attosecond pulse generation on plasma mirrors: basic mechanisms, J. Phys. B At. Mol. Opt. Phys. 43 (2010) 213001. https://doi.org/10.1088/0953-4075/43/21/213001.

[4] P. Yeates, E.T. Kennedy, Plasma dynamics of a confined extreme ultraviolet light source, Phys. Plasmas. 17 (2010) 093104. https://doi.org/10.1063/1.3484227.

[5] C. Aragón, J.A. Aguilera, Characterization of laser induced plasmas by optical emission spectroscopy: A review of experiments and methods, Spectrochim. Acta - Part B At. Spectrosc. 63 (2008) 893–916. https://doi.org/10.1016/j.sab.2008.05.010.

[6] W. Wang, M.M. Fejer, R.H. Hammond, M.R. Beasley, C.H. Ahn, M.L. Bortz, T. Day, Atomic absorption monitor for deposition process control of aluminum at 394 nm using frequency-doubled diode laser, Appl. Phys. Lett. 68 (1996) 729–731. https://doi.org/10.1063/1.116785.

[7] K. Niemax, A. Zybin, C. Schnürer-Patschan, H. Groll, Peer Reviewed: Semiconductor Diode Lasers in Atomic Spectrometry, Anal. Chem. 68 (1996) 351A-356A. https://doi.org/10.1021/ac961942i.

[8] A. Zybin, J. Koch, H.D. Wizemann, J. Franzke, K. Niemax, Diode laser atomic absorption spectrometry, Spectrochim. Acta Part B At. Spectrosc. 60 (2005) 1–11. https://doi.org/10.1016/j.sab.2004.10.001.

[9] K. Niemax, A. Zybin, D. Eger, Peer Reviewed: Tunable Deep Blue Light for Laser Spectrochemistry, Anal. Chem. 73 (2001) 134 A-139 A. https://doi.org/10.1021/ac012409s.

[10] J. Bergevin, T.H. Wu, J. Yeak, B.E. Brumfield, S.S. Harilal, M.C. Phillips, R.J. Jones, Dual-comb spectroscopy of laser-induced plasmas, Nat. Commun. 9 (2018) 1–6. https://doi.org/10.1038/s41467-018-03703-0.

[11] M.G. Tarallo, G.Z. Iwata, T. Zelevinsky, BaH molecular spectroscopy with relevance to laser cooling, Phys. Rev. A. 93 (2016) 032509. https://doi.org/10.1103/PhysRevA.93.032509.

[12] N.L. LaHaye, S.S. Harilal, M.C. Phillips, Early- and late-time dynamics of laser-produced plasmas by combining emission and absorption spectroscopy, Spectrochim. Acta Part B At. Spectrosc. 179 (2021) 106096. https://doi.org/10.1016/j.sab.2021.106096.

[13] S.S. Harilal, E.J. Kautz, R.J. Jones, M.C. Phillips, Spectro-temporal comparisons of optical emission, absorption, and laser-induced fluorescence for characterizing ns and fs laser-produced plasmas, Plasma Sources Sci. Technol. 30 (2021) 045007. https://doi.org/10.1088/1361-6595/abefa5.

[14] G. Hull, E.D. McNaghten, P. Coffey, P. Martin, Isotopic analysis and plasma diagnostics for lithium detection using combined laser ablation–tuneable diode laser absorption spectroscopy and laser-induced breakdown spectroscopy, Spectrochim. Acta - Part B At. Spectrosc. 177 (2021) 106051. https://doi.org/10.1016/j.sab.2020.106051.

[15] M. Ribière, L. Méès, D. Allano, B.G. Chéron, Evolutions in time and space of laser ablated species by dual-laser photoabsorption spectroscopy, J. Appl. Phys. 104 (2008) 043302. https://doi.org/10.1063/1.2960575.

[16] L. Nagli, M. Gaft, I. Gornushkin, Fraunhofer-type absorption lines in double-pulse laser-induced plasma, Appl. Opt. 51 (2012) B201. https://doi.org/10.1364/AO.51.00B201.

[17] S.S. Harilal, B.E. Brumfield, N.L. LaHaye, K.C. Hartig, M.C. Phillips, Optical spectroscopy of laser-produced plasmas for standoff isotopic analysis, Appl. Phys. Rev. 5 (2018) 021301. https://doi.org/10.1063/1.5016053.

[18] M. Miyabe, M. Oba, H. Iimura, K. Akaoka, Y. Maruyama, H. Ohba, M. Tampo, I. Wakaida, Absorption spectroscopy of uranium plasma for remote isotope analysis of next-generation nuclear fuel, Appl. Phys. A. 112 (2013) 87–92. https://doi.org/10.1007/s00339-012-7181-2.

[19] M.C. Phillips, B.E. Brumfield, N. LaHaye, S.S. Harilal, K.C. Hartig, I. Jovanovic, Two-dimensional fluorescence spectroscopy of uranium isotopes in femtosecond laser ablation

plumes, Sci. Rep. 7 (2017) 3784. https://doi.org/10.1038/s41598-017-03865-9.
[20] M. Miyabe, M. Oba, K. Jung, H. Iimura, K. Akaoka, M. Kato, H. Otobe, A. Khumaeni, I. Wakaida, Laser ablation absorption spectroscopy for isotopic analysis of plutonium: Spectroscopic properties and analytical performance, Spectrochim. Acta Part B At. Spectrosc. 134 (2017) 42–51. https://doi.org/10.1016/j.sab.2017.05.008.
[21] L.A. King, I.B. Gornushkin, D. Pappas, B.W. Smith, J.D. Winefordner, Rubidium isotope measurements in solid samples by laser ablation-laser atomic absorption spectroscopy, Spectrochim. Acta - Part B At. Spectrosc. 54 (1999) 1771–1781. https://doi.org/10.1016/S0584-8547(99)00140-8.
[22] B.A. Bushaw, M.L. Alexander, Investigation of laser ablation plume dynamics by high-resolution time-resolved atomic absorption spectroscopy, Appl. Surf. Sci. 127–129 (1998) 935–940. https://doi.org/10.1016/S0169-4332(97)00769-1.
[23] B.A. Bushaw, N.C. Anheier, Isotope ratio analysis on micron-sized particles in complex matrices by Laser Ablation-Absorption Ratio Spectrometry, Spectrochim. Acta Part B At. Spectrosc. 64 (2009) 1259–1265. https://doi.org/10.1016/j.sab.2009.10.002.
[24] J.T. Costello, J.P. Mosnier, E.T. Kennedy, P.K. Carroll, G. O'sullivan, X-uv absorption spectroscopy with laser-produced plasmas: A review, Phys. Scr. 1991 (1991) 77–92. https://doi.org/10.1088/0031-8949/1991/T34/011.
[25] S. Gurlui, M. Agop, P. Nica, M. Ziskind, C. Focsa, Experimental and theoretical investigations of a laser-produced aluminum plasma, Phys. Rev. E. 78 (2008) 026405. https://doi.org/10.1103/PhysRevE.78.026405.
[26] C. Ursu, P. Nica, B.G. Rusu, C. Focsa, V-shape plasma generated by excimer laser ablation of graphite in argon: Spectroscopic investigations, Spectrochim. Acta Part B At. Spectrosc. 163 (2020) 105743. https://doi.org/10.1016/j.sab.2019.105743.
[27] P. Nica, C. Ursu, C. Focsa, Electrical characterization of carbon plasma generated by excimer laser ablation of graphite, Appl. Surf. Sci. 540 (2021) 148412. https://doi.org/10.1016/j.apsusc.2020.148412.
[28] C. Focsa, S. Gurlui, P. Nica, M. Agop, M. Ziskind, Plume splitting and oscillatory behavior in transient plasmas generated by high-fluence laser ablation in vacuum, Appl. Surf. Sci. 424 (2017) 299–309. https://doi.org/10.1016/j.apsusc.2017.03.273.
[29] P.-E. Nica, M. Agop, S. Gurlui, C. Bejinariu, C. Focsa, Characterization of Aluminum Laser Produced Plasma by Target Current Measurements, Jpn. J. Appl. Phys. 51 (2012) 106102. https://doi.org/10.1143/JJAP.51.106102.
[30] C. Ursu, O.G. Pompilian, S. Gurlui, P. Nica, M. Agop, M. Dudeck, C. Focsa, Al2O3 ceramics under high-fluence irradiation: plasma plume dynamics through space- and time-resolved optical emission spectroscopy, Appl. Phys. A. 101 (2010) 153–159. https://doi.org/10.1007/s00339-010-5775-0.
[31] R.F. Wood, K.R. Chen, J.N. Leboeuf, a. A. Puretzky, D.B. Geohegan, Dynamics of Plume Propagation and Splitting during Pulsed-Laser Ablation, Phys. Rev. Lett. 79 (1997) 1571–1574. https://doi.org/10.1103/PhysRevLett.79.1571.
[32] R.F. Wood, J.N. Leboeuf, D.B. Geohegan, A.A. Puretzky, K.R. Chen, Dynamics of plume propagation and splitting during pulsed-laser ablation of Si in He and Ar, Phys. Rev. B. 58 (1998) 1533–1543. https://doi.org/10.1103/PhysRevB.58.1533.
[33] J. Wu, X. Li, W. Wei, S. Jia, A. Qiu, Understanding plume splitting of laser ablated plasma: A view from ion distribution dynamics, Phys. Plasmas. 20 (2013). https://doi.org/10.1063/1.4835255.
[34] C. Focsa, P. Nemec, M. Ziskind, C. Ursu, S. Gurlui, V. Nazabal, Laser ablation of AsxSe100-x chalcogenide glasses: Plume investigations, Appl. Surf. Sci. 255 (2009) 5307–5311. https://doi.org/10.1016/j.apsusc.2008.07.204.
[35] K.K. Anoop, X. Ni, X. Wang, S. Amoruso, R. Bruzzese, Fast ion generation in femtosecond laser ablation of a metallic target at moderate laser intensity, Laser Phys. 24 (2014) 105902. https://doi.org/10.1088/1054-660X/24/10/105902.
[36] K.K. Anoop, S.S. Harilal, R. Philip, R. Bruzzese, S. Amoruso, Laser fluence dependence on emission dynamics of ultrafast laser induced copper plasma, J. Appl. Phys. 120 (2016) 185901. https://doi.org/10.1063/1.4967313.

[37] N.M. Bulgakova, A. V. Bulgakov, O.F. Bobrenok, Double layer effects in laser-ablation plasma plumes, Phys. Rev. E - Stat. Physics, Plasmas, Fluids, Relat. Interdiscip. Top. 62 (2000) 5624–5635. https://doi.org/10.1103/PhysRevE.62.5624.
[38] M. Miyabe, M. Oba, H. Iimura, K. Akaoka, Y. Maruyama, H. Ohba, M. Tampo, I. Wakaida, Doppler-shifted optical absorption characterization of plume-lateral expansion in laser ablation of a cerium target, J. Appl. Phys. 112 (2012) 123303. https://doi.org/10.1063/1.4771879.
[39] K.H. Song, X. Xu, Mechanisms of absorption in pulsed excimer laser-induced plasma, Appl. Phys. A Mater. Sci. Process. 65 (1997) 477–485. https://doi.org/10.1007/s003390050612.
[40] S.S. Harilal, E.J. Kautz, M.C. Phillips, Spatiotemporal evolution of emission and absorption signatures in a laser-produced plasma, J. Appl. Phys. 131 (2022) 063101. https://doi.org/10.1063/5.0081597.
[41] C. Ursu, S. Gurlui, C. Focsa, G. Popa, Space- and time-resolved optical diagnosis for the study of laser ablation plasma dynamics, Nucl. Instruments Methods Phys. Res. Sect. B Beam Interact. with Mater. Atoms. 267 (2009) 446–450. https://doi.org/10.1016/j.nimb.2008.10.057.
[42] C. Ursu, P. Nica, C. Focsa, Excimer laser ablation of graphite: The enhancement of carbon dimer formation, Appl. Surf. Sci. 456 (2018) 717–725. https://doi.org/10.1016/j.apsusc.2018.06.217.
[43] O. Axner, J. Gustafsson, N. Omenetto, J.D. Winefordner, Line strengths, A-factors and absorption cross-sections for fine structure lines in multiplets and hyperfine structure components in lines in atomic spectrometry—a user's guide, Spectrochim. Acta Part B At. Spectrosc. 59 (2004) 1–39. https://doi.org/10.1016/j.sab.2003.10.002.
[44] E.S. Chang, Energy Levels of Atomic Aluminum with Hyperfine Structure, J. Phys. Chem. Ref. Data. 19 (1990) 119–125. https://doi.org/10.1063/1.555870.
[45] S.S. Harilal, E.J. Kautz, M.C. Phillips, Time-resolved absorption spectroscopic characterization of ultrafast laser-produced plasmas under varying background pressures, Phys. Rev. E. 103 (2021) 013213. https://doi.org/10.1103/PhysRevE.103.013213.
[46] P. Hannaford, The Oscillator Strength in Atomic Absorption Spectroscopy, Microchem. J. 63 (1999) 43–52. https://doi.org/10.1006/mchj.1999.1766.
[47] M. Wolter, H.T. Do, H. Steffen, R. Hippler, Aluminium atom density and temperature in a dc magnetron discharge determined by means of blue diode laser absorption spectroscopy, J. Phys. D. Appl. Phys. 38 (2005) 2390–2395. https://doi.org/10.1088/0022-3727/38/14/014.
[48] S. Sunil, A. Kumar, R.K. Singh, K.P. Subramanian, Measurements of electron temperature and density of multi-component plasma plume formed by laser-blow-off of LiF-C film, J. Phys. D. Appl. Phys. 41 (2008) 85211. https://doi.org/10.1088/0022-3727/41/8/085211.
[49] I. Weaver, G.W. Martin, W.G. Graham, T. Morrow, C.L.S. Lewis, The Langmuir probe as a diagnostic of the electron component within low temperature laser ablated plasma plumes, Rev. Sci. Instrum. 70 (1999) 1801–1805. https://doi.org/10.1063/1.1149672.
[50] David Salzmann, Atomic Physics in Hot Plasmas, Oxford University Press, Oxford, 1998.
[51] P.-E. Nica, S. Miyamoto, S. Amano, T. Inoue, A. Shimoura, K. Kaku, T. Mochizuki, Soft x-ray spectra from laser heated lithium targets, Appl. Phys. Lett. 89 (2006) 041501. https://doi.org/10.1063/1.2235956.
[52] H.R. Griem, G. Hans R., Principles of Plasma Spectroscopy, Cambridge University Press, Cambridge, 2005.
[53] H.R. Griem, Spectral line broadening by plasmas, Academic Press, New York, London, 1974.
[54] S. Amoruso, R. Bruzzese, N. Spinelli, R. Velotta, Characterization of laser-ablation plasmas, J. Phys. B At. Mol. Opt. Phys. 32 (1999) R131–R172. https://doi.org/10.1088/0953-4075/32/14/201.
[55] R. Mitzner, A. Rosenfeld, R. König, Time-resolved absorption studies of excimer laser ablation of CaF2, Appl. Surf. Sci. 69 (1993) 180–184. https://doi.org/10.1016/0169-4332(93)90501-2.
[56] C. Ursu, P. Nica, B.G. Rusu, C. Focsa, V-shape plasma generated by excimer laser ablation of graphite in argon: Spectroscopic investigations, Spectrochim. Acta - Part B At. Spectrosc. 163 (2020). https://doi.org/10.1016/j.sab.2019.105743.
[57] A. Lesage, Experimental Stark widths and shifts for spectral lines of neutral and ionized atoms A critical review of selected data for the period 2001–2007, New Astron. Rev. 52 (2009) 471–

535. https://doi.org/10.1016/j.newar.2008.01.001.
[58] J.J. Shea, A plasma formulary for physics, technology, and astrophysics [Book Review], IEEE Electr. Insul. Mag. 19 (2003) 52–52. https://doi.org/10.1109/MEI.2003.1178121.
[59] I.B. Gornushkin, L.A. King, B.W. Smith, N. Omenetto, J.D. Winefordner, Line broadening mechanisms in the low pressure laser-induced plasma, Spectrochim. Acta Part B At. Spectrosc. 54 (1999) 1207–1217. https://doi.org/10.1016/S0584-8547(99)00064-6.
[60] J. Olejnicek, H.T. Do, Z. Hubicka, R. Hippler, L. Jastrabik, Blue Diode Laser Absorption Spectroscopy of Pulsed Magnetron Discharge, Jpn. J. Appl. Phys. 45 (2006) 8090–8094. https://doi.org/10.1143/JJAP.45.8090.
[61] H. Scheibner, S. Franke, S. Solyman, J.F. Behnke, C. Wilke, A. Dinklage, Laser absorption spectroscopy with a blue diode laser in an aluminum hollow cathode discharge, Rev. Sci. Instrum. 73 (2002) 378–382. https://doi.org/10.1063/1.1430548.
[62] C. Vitelaru, V. Pohoata, C. Aniculaesei, V. Tiron, G. Popa, The break-down of hyperfine structure coupling induced by the Zeeman effect on aluminum 2S1/2→2P1/2 transition, measured by tunable diode-laser induced fluorescence, J. Appl. Phys. 109 (2011) 084911. https://doi.org/10.1063/1.3579446.
[63] T. Fujimoto, R.W.P. McWhirter, Validity criteria for local thermodynamic equilibrium in plasma spectroscopy, Phys. Rev. A. 42 (1990) 6588–6601. https://doi.org/10.1103/PhysRevA.42.6588.
[64] G. Cristoforetti, A. De Giacomo, M. Dell'Aglio, S. Legnaioli, E. Tognoni, V. Palleschi, N. Omenetto, E. Tognoni, V. Palleschi, M. Dell'Aglio, S. Legnaioli, G. Cristoforetti, A. De Giacomo, Local Thermodynamic Equilibrium in Laser-Induced Breakdown Spectroscopy: Beyond the McWhirter criterion, Spectrochim. Acta Part B At. Spectrosc. 65 (2010) 86–95. https://doi.org/10.1016/j.sab.2009.11.005.